IN-20

13P

NASA Contractor Report 194471
IEPC–93–097

Stationary Plasma Thruster Plume Emissions

David H. Manzella
Sverdrup Technology, Inc.
Lewis Research Center Group
Brook Park, Ohio

Prepared for the
23rd International Electric Propulsion Conference
sponsored by the American Institute of Aeronautics and Astronautics
Seattle, Washington, September 13–16, 1993

National Aeronautics and
Space Administration

(NASA-CR-194471) STATIONARY PLASMA THRUSTER PLUME EMISSIONS Final Report (Sverdrup Technology) 13 p

N94-26209

Unclas

G3/20 0208980

Stationary Plasma Thruster Plume Emissions

David H. Manzella
Sverdrup Technology Inc.
Lewis Research Center Group
Brook Park, Ohio 44142

The emission spectrum from a xenon plasma produced by a Stationary Plasma Thruster provided by the Ballistic Missile Defense Organization (BMDO) was measured. Approximately 270 individual Xe I, Xe II, and Xe III transitions were identified. A total of 250 mW of radiated optical emission was estimated from measurements taken at the thruster exit plane. There was no evidence of erosion products in the emission signature. Ingestion and ionization of background gas at elevated background pressure was detected. The distribution of excited states could be described by temperatures ranging from fractions of 1 eV to 4 eV with a high degree of uncertainty due to the non-equilibrium nature of this plasma. The plasma was over 95% ionized at the thruster exit plane. Between 10 and 20% of the ions were doubly charged. Two modes of operation were identified. The intensity of plasma emission increased by a factor of two during operation in an oscillatory mode. The transfer between the two modes of operation was likely related to unidentified phenomena occurring on a time scale of minutes.

Introduction

The stationary plasma thruster (SPT) developed in the former Soviet Union over the past several decades offers performance levels attractive to western spacecraft manufacturers for north-south station-keeping.[1] In order to more fully assess the suitability of this technology for fulfilling such mission requirements, the NASA Lewis Research Center (LeRC) has begun evaluating performance and integration issues using an SPT provided by the Ballistic Missile Defense Organization (BMDO).[2-5] Integration issues include the impact of the thruster induced plasma environment on spacecraft subsytems. These impacts may be estimated based on measurements of SPT plasma properties in an appropriate altitude simulation chamber.

The energetic xenon plasma produced by the SPT is sustained within an annular discharge chamber by an axial electric field established between an external hollow cathode and an anode located at the rear. The acceleration of the ions formed in the discharge chamber by the electric field provides thrust. A unique aspect of the SPT is the interaction between the axial electric field and a radial magnetic field established by electromagnets which imparts a circumferential force on the magnetized electrons and decreases their axial electron conductivity. Collisional processes involving the electrons dominate many of the phenomena which determine the thermo-chemical state of the exiting plasma. However, complete specification of the characteristics of the plasma jet as it exits the discharge chamber requires knowledge of the alignment and strength of the electric and magnetic fields, the type and frequency of interactions of the plasma constituents with one another and the dielectric thruster walls, and the interaction of the thruster efflux with the ambient environment.

The complexity of the various processes mentioned above currently precludes the use of analytic or numerical methods for predicting this behavior and, in spite of an extensive flight history for the SPT-70 (the 70 designates the exit diameter in mm),[6] integration of these engines onto western satellites still requires assessment of the potential impacts of the exhaust on various subsystems.[7] Experimental measurements of the SPT plasma using electrostatic probes have provided data on the charged particles in the plume.[8-15] However, in some cases optical diagnostics can provide detailed, specie-specific, non-intrusive measurements on neutral particles and ions. Optical measurements have been made by several SPT investigators.[15-17] The BMDO sponsored assessment of the SPT at LeRC includes optical diagnostics for the measurement of the plasma characteristics in the SPT-100's plume. This report describes the current status of an investigation of the plume using emission spectroscopy.

Nomenclature

A_{ik}	transition probability from state i to k, s^{-1}
E_i	energy of state i, J
g_i	degeneracy of state i
$I(\nu)$	spectral intensity, $W/m^2 \cdot sr \cdot s^{-1}$
$I_m(\nu)$	measured spectral intensity, $W/m^2 \cdot sr \cdot s^{-1}$
k	Boltzmann's constant, J/K
$k(\nu)$	spectral absorption coefficient, m^{-1}
L	spatial extent of plasma, m
n	number density, m^{-3}
n_i	number density of state i, m^{-3}
Q_{el}	electronic partition function
T	temperature, K
$T(\nu)$	radiation transmission function, s
z	spatial coordinate, m
$\varepsilon(\nu)$	spectral emission coefficient, $W/m^3 \cdot sr \cdot s^{-1}$
$\phi(\nu)$	spectral line shape function, s
ν	frequency, s^{-1}
ν_o	transition frequency, s^{-1}

Analyses

One can infer information on the state of a plasma by interpreting the spectra of the light radiated by that plasma. One mechanism which produces this radiation is spectral line emission which occurs when excited plasma constituents spontaneously decay to lower energy states. The intensity of the light emitted from one of these transitions can be related to the population of the excited state whose decay gives rise to the spectral line. This is accomplished through a solution to the one dimensional equation of radiative transfer.

$$\frac{dI}{dz} = \varepsilon(\nu,z) - k(\nu,z)\, I(\nu,z) \qquad (1)$$

This equation can be integrated from z = 0 to z = L for a homogeneous plasma of known extent.

$$I(\nu,L) = \frac{\varepsilon(\nu)}{k(\nu)}[1-\exp(-k(\nu)L] + I(\nu,0)\exp(-k(\nu)L) \qquad (2)$$

For an optically thin plasma, *i.e.* $k(\nu)L << 1$, with negligible incident radiation, the intensity of the light emitted by the plasma is directly proportional to the spectral emission coefficient.

$$I(\nu,L) = \varepsilon(\nu)\, L \qquad (3)$$

Considering only line emission, the spectral emission coefficient can be related directly to the number density of the excited state whose spontaneous decay results in the spectral line. For this case equation (3) becomes:

$$I(\nu,L) = \frac{h\nu}{4\pi} A_{ik}\, n_i\, \phi(\nu)\, L \qquad (4)$$

This relation can be used to determine the excited state number density if the frequency dependent spectral intensity can be measured. However, it was not possible to directly measure the frequency dependent spectral intensity in this investigation because measurements were made with an instrument which had a non-negligible radiation transmission function. Therefore, the observed intensities can be represented as a convolution of equation (4) and an appropriate radiation transmission function, $T(\nu)$.[18] For this case equation (4) becomes:

$$\int_0^{\infty} I(\nu^*,L)\, T(\nu-\nu^*)\, d\nu^* = \frac{h\nu}{4\pi} A_{ik}\, n_i\, L \int_0^{\infty} \phi(\nu^*) T(\nu-\nu^*)\, d\nu^* \qquad (5)$$

When the transmission function is wide and approximately constant in the frequency range corresponding to the spectral line shape function, the integral on the right hand side of this equation can be evaluated. The left hand side of the equation is the measured intensity, which is the convolution of the emitted intensity and the transmission function. Therefore, the number density of state *i* can be determined from the measured intensity providing the transition probability is known.

$$n_i = \frac{4\pi}{h\nu} \frac{I_m(\nu,L)}{A_{ik}\, L\, T(\nu-\nu_0)} \qquad (6)$$

To determine the plasma conditions based on the number density of excited states, one needs to consider the mechanisms responsible for populating these states. The populations of all the excited states are determined by various collisional and radiative processes occurring in the plasma. When the forward rates of all collisional processes are balanced by their reverse rates, a plasma is said to be in local thermodynamic equilibrium. For this case the distribution of excited states can be described by the plasma temperature based on Boltzmann statistics.[19]

$$\frac{n_i}{n} = \frac{g_i \exp(-E_i/kT)}{Q_{el}} \qquad (7)$$

Furthermore, based on the temperature and total atom number density a Saha relation can be used to determine the ion and electron density.[19]

Past investigations into the SPT plasma have suggested that not all states exhibit this type of equilibrium behavior and that ground state collisional excitation and radiative decay of excited states are the mechanisms responsible for determining the distribution of excited states.[10-12] This type of equilibrium is often referred to as corona equilibrium. The existence of several long lived metastable states of Xe I such as the $6s[3/2]_2$ and $6s'[1/2]_0$ levels which have radiative lifetimes of 150 sec and 78 msec respectively[20] suggest collisional processes involving these states may also be important.

A collisional-radiative equilibrium (CRE) model based on the rates of the individual exciting and depopulating mechanism could be used to interpret the number density of excited states if collisional and radiative processes are both dominant relative to convective transport in the SPT plasma. Collisional and radiative rates can be calculated based on transition probabilities, collision cross sections, and a suitable electron energy distribution function. A CRE model was constructed in this fashion to interpret the spectra of a hydrogen arcjet.[21]

While a CRE model may be the appropriate model to describe the distribution of excited states in an SPT produced xenon plasma, no such model was developed during the course of this investigation for several reasons. First, the atomic structure of xenon makes a CRE model of the SPT far more complex than hydrogen. Figure 1 is a partial Grotrian energy

level diagram for xenon constructed from published energy levels.[22] This shows the splitting of states with the same principal quantum number due to spin-orbit coupling of the valence electrons. Since a CRE model requires a rate equation for each level, the number of states for xenon necessitates a very large matrix of equations or appropriate lumping of multiple states to reduce the number of coupled, nonlinear differential equations. The collision cross sections needed to determine the rates for the various processes considered in a CRE model can often be calculated based on an oscillator strength and an electron energy distribution function. However, many xenon oscillator strengths remain unknown. Additionally, while investigations of the electron energy distribution function in SPTs have been conducted,[9,15] there remains a large degree of uncertainty as to the appropriate distribution function. Future work is required to the resolve these issues in hopes of developing a xenon CRE model if warranted.

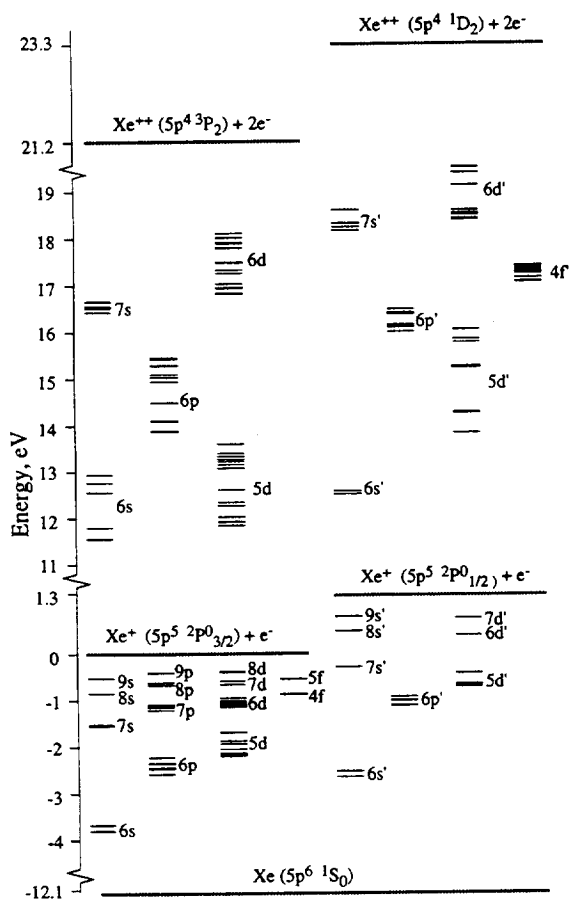

Figure 1: Partial Xenon Energy Level Diagram

Experimental

An experimental apparatus was implemented to take spectroscopic measurements of the plasma produced by the Russian SPT-100 thruster. Preliminary data were taken concurrently with performance measurements in Vacuum Facility 5 of the Electric Propulsion Laboratory at the NASA Lewis Research Center. The 19 m long and 5 m diameter cylindrical chamber was cryogenically pumped with two 41 m^2 helium cryopanels installed at one end of the chamber partially separated from the remainder of the tank by an auxiliary baffle and movable louvers. These louvers were in the open position during operation. The pumping system's twenty, 0.8 m diameter oil diffusion pumps were not employed. The thruster was mounted on a thrust balance in a 1 m diameter test port that could be isolated from the main chamber with a gate valve. The configuration for these tests is shown in Figure 2.

The effect of chamber pressure on operation was considered during performance evaluations. The tank pressure was varied by introduction of either nitrogen or xenon into the main chamber for these tests. The pressure was monitored using two hot-cathode ionization gauges. One gage was located in the test port. The other was located in the main chamber. During thruster operation the tank pressure ranged from 1×10^{-4} Torr to 3×10^{-6} Torr.

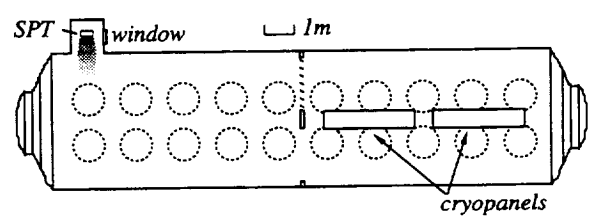

Figure 2. - Tank 5 including SPT and cryopanels

The remainder of the spectroscopic measurements were taken with the SPT operating in Vacuum Facility 8 of the Electric Propulsion Laboratory. The 5 m long by 1.5 m diameter cylindrical chamber depicted in Figure 3 was pumped by four 0.82 m oil diffusion pumps, a lobe type mechanical blower, and two piston type roughing pumps. The thruster was mounted in a 0.6 m diameter test port. The ambient pressure as measured by an ionization gauge during testing was 3×10^{-5} torr in the main chamber and 6×10^{-5} torr in the test port.

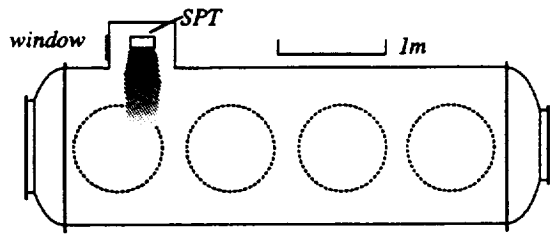

Figure 3: Tank 8 with SPT

In both cases optical measurements were taken through a window located on the test port to permit transverse viewing of the exhausting plasma. The transmissivity of this window declined significantly at wavelength below 3500 Å. A 80 mm x 0.08 mm cross sectional slice of the plasma at the thruster exit was collimated using a 25 mm diameter achromatic lens. The collimated beam was directed to a 0.5 m Czerny-Turner scanning monochromator using front surface mirrors where it was focused onto the entrance slit using a 25 mm diameter achromatic lens. For the preliminary measurements in Tank 5 the collimating lens had a 600 mm focal length and the focusing lens had a 200 mm focal length. Tank 8 measurements were conducted with a 400 mm focal length collimating lens and a 100 mm focusing lens. A simplified schematic of this detection scheme is shown in Figure 4.

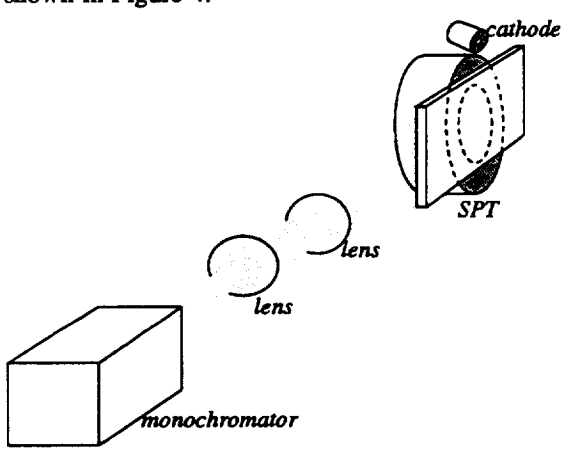

Figure 4: Simplified Schematic of the Optical Path for Emission Measurements

The 0.5 m monochromator's grating was 64 x 64 mm, had 1200 grooves/mm, and was blazed for maximum throughput at 5000 Å. The reciprocal linear dispersion was 17 Å/mm. The transmission function of this system was determined to be Gaussian in shape with a full-width-at-half-maximum of 4.5 Å. The photodetector was a 28 mm diameter, red and blue sensitive, side-on, photomultiplier tube (PMT) biased to 1000 Volts. Phase sensitive detection was employed to discriminate against light from sources other than the SPT. An optical chopper operating at 400 Hz was located in front of the collimating lens. The PMT anode current was converted to a voltage across a 10 kΩ load resistor and measured using a lock-in amplifier phase locked to the optical chopper. The lock-in amplifier was operated with a 100 millisecond time constant. For the majority of scans a long pass interference filter with a 5500 Å cut-off was used at wavelengths above 7000Å to avoid second order spectra.

The SPT-100 thruster provided by BMDO was fabricated in Russia. A description of the internal construction of the thruster can be found elsewhere.[23] The inner and outer diameters of the annular discharge chamber were 56 and 100 mm. The external hollow cathode, mounted in the 12 o'clock position during the majority of the tests, was heated by an internal heater prior to start up. A laboratory model power supply, designed and built at Lewis, was used to run the thruster and operate the cathode heater.[3] For tests conducted in Tank 8 the thruster operated at the conditions shown in Table I. These values are compared to values obtained during similar tests conducted by Fakel Enterprises in Kaliningrad, Russia.[24] All tests were conducted using commercially available research grade xenon (99.9995% pure) as the propellant. A complete performance characterization of this thruster can be found in Reference 2.

Table I: SPT-100 Operating Conditions

Quantity, units	LeRC	Fakel
Total Xenon Flow Rate, sccm	47.4	49.6
Thruster Voltage, volts	296.8	300
Discharge Current, amps	4.38	4.35
Thruster Power, watts	1300	1305
Cathode to Ground Voltage, volts	21.4	21.1

For each test the thruster was allowed to run for a minimum of ten minutes to establish steady state prior to taking spectroscopic measurements. Emission measurements were obtained by scanning the monochromator from 3000 to 9000 Å at a rate of 1 Å/s. During the emission measurements taken in Tank 5 the thruster operating conditions were varied as the performance characteristics were measured. These changes in operating conditions were reflected in changes in the measured intensities. Subsequent dedicated tests were conducted at a one operating condition.

In several instances during steady state thruster operation the thruster transitioned from a quiescent mode characterized by nearly constant discharge current to a oscillatory mode characterized by significant current oscillations. The transition between modes was abrupt and unanticipated. The temporal behavior of the thruster power is displayed for each of the modes in Figure 5. The 12 kilohertz oscillation in the thruster power was primarily the result of a 4 Amp peak to peak variation in the discharge current. The regular high frequency spikes were indicative of the power processing unit's 40 kHz switching transients. All spectroscopic data reported in the following section were taken while the thruster operated in a quiescent mode unless otherwise indicated.

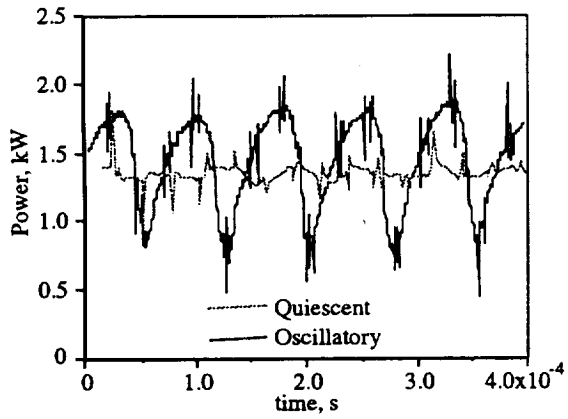

Figure 5: Time Dependent Behavior of Thruster Power in the Quiescent and Oscillatory Modes.

After measuring the emission spectra from the SPT an in situ intensity calibration of the spectroscopic system was conducted. The SPT was removed from the test port and a tungsten ribbon lamp at 2300 K was placed in the same location. Gray body continuum radiation was measured using the spectroscopic system with no modifications. The emissive power of the filament image on the detector was calculated using a Planck function and published values for the emissivity of tungsten.[25] The estimated uncertainty in this calibration was less than ten percent.

Results and Discussion

The measured emission spectrum from the exit plane of the SPT-100 is shown in Figure 6. Approximately 270 individual atomic and ionic transitions were identified based on tabulated data.[26] The majority of the emission occurred in the blue part of the spectrum between 4200 and 5000 Å. This was primarily due to Xe II, the singly ionized xenon ion. Over the entire spectral region measured, neutral xenon atom emission lines were of lesser but comparable intensity to the Xe II emission lines. The most prominent emission lines from doubly ionized xenon, Xe III, which were in the UV, were also detected. These Xe III lines were weaker in intensity. No continuum radiation was measured. The measured line shapes were primarily instrument broadened prohibiting spectral line analysis. No emission was measured below 3500 Å due to the decreased transmissivity of the window at these wavelengths.

In addition to emission from various configurations of xenon, emission from other species was considered. Specifically, because the SPT insulator erodes during operation, optical detection of atomic erosion products was investigated. Based on the composition of the insulator, the strongest transitions from neutral and singly ionized B, N, Si, and O were considered. The wavelengths of these transitions are listed in Table II. There was no evidence of emission from these species. Subsequent calculations based on a published end of life volume erosion measurements[7] were consistent with the experimental data. Based on the known volume erosion rate a constant mass erosion rate of 27 mg/hr was estimated, permitting calculation of the flux of erosion products at the thruster exit. Assuming a 20 km/s velocity for these constituents a number density of the erosion products on the order of 10^{14} m^{-3} was determined. If the distribution of excited states can be described using Boltzmann statistics and a distribution temperature of 1 eV, even the most intense Si II line is an order of magnitude below the detectability limit. Improvements in the spectroscopic system to increase the sensitivity are possible and may be considered for future tests.

Table II: Spectral Lines of Potential Erosion Products: Boron, Nitrogen, Silicon, and Oxygen (Reference 27).

Species	Wavelength, Å
B II	3451.3
N II	3995.0
O II	4075.9
B II	4121.9
O II	4189.8
O II	4649.1
N II	4630.5
N II	5005.2
Si II	5041.0
Si II	5056.0
N II	5679.6
O I	6158.2
Si II	6347.1
Si II	6371.4
N I	7468.3
O I	7771.9
O I	7774.2
O I	7775.4

During performance testing in Tank 5 the facility background pressure was increased to 10^{-4} Torr by a controlled flow of nitrogen into the vacuum tank. During these series of tests, spectroscopic measurements were taken in the 8000 - 9000 Å range without a long pass interference filter. Many transitions previously measured were recorded in second order. In addition to the second order xenon transitions, molecular emission from singly ionized molecular nitrogen was measured. The $B^2\Sigma_u \leftarrow X^2\Sigma_g$ (0,1) transition of N_2^+ at 4278.8 was the most intense of these transitions. This was clear evidence that there was ionization of the background gas within the SPT produced plasma. An estimation of the mass flux of 300 K nitrogen at 10^{-4} Torr based on kinetic theory suggests that an amount of background nitrogen equivalent to approximately 2% of the supplied mass flow was ingested through the exit plane of the thruster. If this ingested mass were ionized within the discharge chamber and accelerated by the applied electric field there would be a measurable effect on thrust. There would be no way to distinguish ingested mass when the background

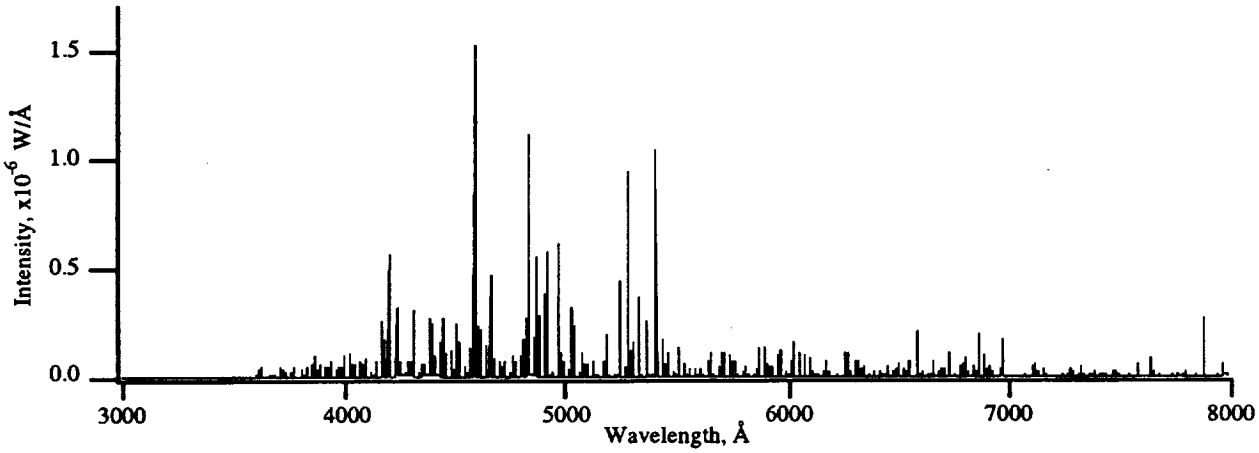

Figure 6: Measured Emission Spectrum at Thruster Exit Plane

was the propellant gas. The effect of facility pressure on performance is discussed in Reference 2.

To determine the brightness of the SPT plume the measured emission spectra was integrated with respect to wavelength. Approximately 0.2 mW of light was emitted by the 80 micron thick slice of plasma at the thruster exit plane. In order to estimate the total power emitted by the plume, this result was extrapolated assuming a homogeneous plasma one exit plane diameter in axial extent. The amount of power emitted from within this volume was 230 mW. This excludes the power emitted by the plasma in the discharge chamber and the power lost through resonance transitions in the vacuum ultraviolet (VUV). These transitions were not measured at this time due to the increased experimental complexity of making VUV emission measurements.

Based on the measured intensities, the number density path length product was determined using equation (6) for those transitions with an unambiguously determined intensity and a known transition probability. The intensity of several transitions could not be determined due to the close proximity of other transitions and limited spectral resolution. The designation of the transitions considered for this analysis, the wavelength (in air), the energy of the upper and lower states, the degeneracy of each state, the published transition probabilities, and the experimentally determined number densities are included in the Appendix.

In order to determine plasma conditions based on the number density of excited states a description of the equilibrium model was needed. The utility of Boltzmann statistics, which implies collisional equilibration among excited states and a Maxwellian electron energy distribution, was considered. Boltzmann plots for Xe II and Xe I are shown in Figures 7 and 8. These figures show the quantity n_iL divided by the degeneracy of state i plotted on a log scale versus E_i. The uncertainties are primarily due to uncertainties in the transition probabilities. Those points without error bars were determined using calculated transition probabilities.

If the plasma were in Boltzmann equilibrium each of these points would fall on a line with a slope of -1/kT according to equation (7) . Even if electron collision frequencies were not adequate to maintain such an equilibrium for all excited states, states close in energy to the ionization continuum may still be in equilibrium with an excited state distribution reflecting the electron temperature. While the measured distribution shown for Xe II is bounded by values of kT between 0.45 and 3.9 eV, the scatter indicates that collisional phenomena do not dominate the processes giving rise to the distribution of the excited states measured. Similarly, the fact that there are levels populated which are not coupled to the ground state by an optically allowed transition indicates that a corona type equilibrium is also inappropriate. Therefore, a plasma model taking into account both collisional and radiative processes would be needed for an accurate description of the excited state distribution.

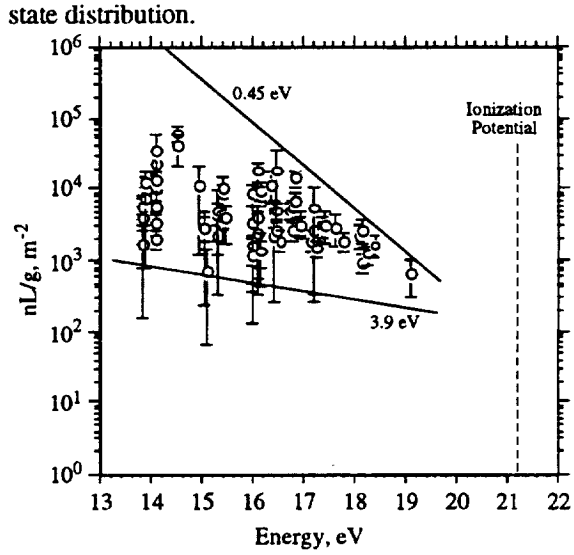

Figure 7: Boltzmann Plot for Xe II

The levels whose excited state populations were suppressed were generally from a manifold of states coupled to the ground state via strong resonant radiative transitions or close in energy to a manifold of states collisionally coupled to the ground state via strong resonant radiative transitions. Because states close in energy are more likely to be collisionally coupled than states spaced further in energy, this can provide an efficient two step process for depopulating a normally long lived excited state when collisionally coupled to a state which strongly radiates to the ground state.[28] A specific example of this is the 6p manifold of Xe I. The four lowest energy points depicted in Figure 8 are from this manifold. The population of all of these states is suppressed relative to the collisional dominated equilibrium suggested by the other states. The $6p[1/2]_1$ state is strongly coupled to the ground through an optically allowed transition. Similarly, as can be seen in Figure 1 the lowest energy state in the 6p manifold is close in energy to a state in the 6s' manifold which is also strongly coupled to ground, providing a rapid depopulating mechanism. The two other states from this manifold are suppressed to a lesser extent, but are still coupled to ground through collisional transfer in the manifold.

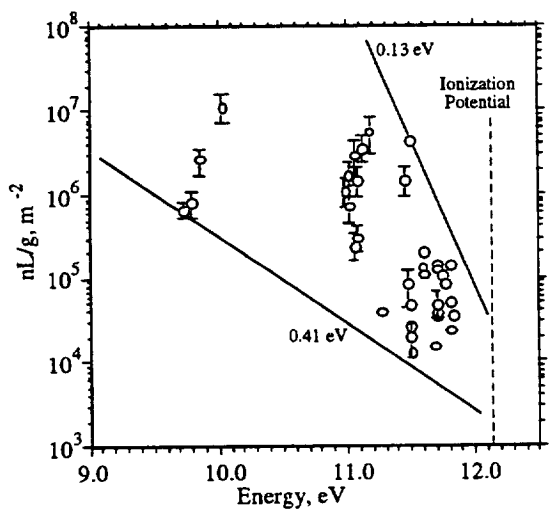

Figure 8: Boltzmann Plot for Xe I

The ionization fractions for singly and doubly ionized xenon were determined based on a total xenon number density of 2.5×10^{17} m^{-3} at the thruster exit plane, estimated from the propellant flow rate and specific impulse, an average geometric optical path length of 54 mm, and the experimentally determined excited state number densities. A representative excited state number density was related to the total number density of that ionization state and the distribution temperature using equation (7). With the assumption of a common distribution temperature, a total of three of these Boltzmann relations, one for each ionization state detected, and an atom balance equation provided a closed set of equations for the total number density of each constituent and the distribution temperature. The calculated common distribution temperature was 0.7 eV and the composition of the plasma was <1% Xe I, 89% Xe II, and 11.9% Xe III. This ionization fraction was consistent with a previous report which indicated an ionization fraction in the discharge chamber above 0.95.[7]

While the result of this calculation was insensitive to the optical path length, deviations from Boltzmann equilibrium for a low pressure, recombining plasma with ground state resonance radiation trapped, would have resulted in an under predicted temperature. Doubling the distribution temperature to 1.4 eV, a more reasonable value based on the Xe II Boltzmann plot and probe measurements taken downstream of the exit plane,[5] resulted in a plasma composition of 5% Xe I, 76% Xe II, and 19 % Xe III. While it was not possible to calculate the uncertainties, it seems likely that no more than 5% of the plasma at the exit of the discharge chamber remains neutral, and that less than 20% of the ions are doubly charged.

The excited state populations for each of the various species normalized by the estimated line of sight averaged total number density and the appropriate degeneracy and partition function are shown in Figure 9. The distribution of excited state number densities for Xe II and Xe III appear self consistent while the Xe I distribution reflects a relatively lower temperature. As previously mentioned the scatter among the data from an individual species was attributed to a low xenon-electron collision frequency relative to radiative processes. However, the differences between the Xe I distribution relative to Xe II and Xe III are likely due to inhomogeneities along the integrated optical path length. Temperature variations within the optical detection volume were likely. A different distribution of the atoms among the various ionization states within these different temperature regions would result. For example, a less energetic region of plasma adjacent to the walls of the discharge chamber would consist of a disproportionately high amount of atomic xenon relative to a more energetic region near the center of the annular discharge chamber. In this work emission from such a region was indistinguishable from these other regions. In order to investigate this, the spatial variation of the excited state number densities is required. This can be determined from Abel inverting spatial maps of each of the transitions used in such an analysis.

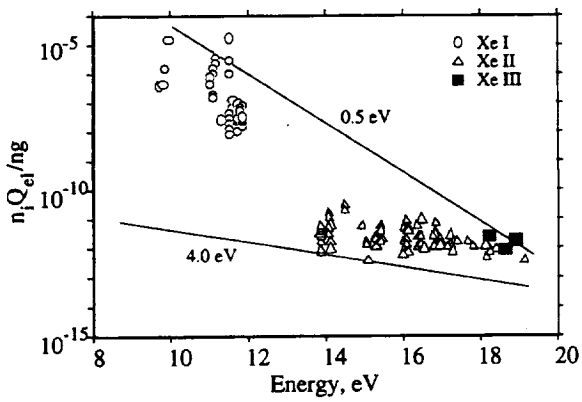

Figure 9: Boltzmann Plot for Xe I, Xe II, and Xe III

These data were all recorded while the thruster was operating in a quiescent mode. Additional data were taken to examine the changes in the plasma emissions while the SPT operated in the oscillatory mode previously described. This was accomplished by monitoring the intensity of one particular atomic or ionic transition as a function of time. While simultaneous tests monitoring both an atomic and ionic line were not performed, the similarity of results for both indicated that the intensity from one line was indicative of the intensity of the entire emission spectrum. No data on the change in the distribution of excited states during operation in the oscillatory mode were taken.

The intensity of the 5419.2 Å Xe II line as a function of time is shown in Figure 10 for two different flow rates. The maximum intensities were measured while the thruster was operating in the oscillatory mode. The minimum intensities, approximately half the maximum value, were measured while the thruster operated in the quiescent mode. The transition from quiescent to oscillatory mode was not immediate. The thruster would intermittently run in each mode and would stay oscillatory for increasing durations until remaining stable in this mode. The cathode to ground floating voltage also decreased from approximately 20 to 19 volts during this transition. The steady state discharge current, and therefore, the average thruster power increased by approximately 5% in the oscillatory mode. However as shown in Figure 5, the instantaneous power may have been as high as 40 % above the quiescent value. Because the phenomena giving rise to electronic excitation are nonlinear with power, the factor of two change in intensity may be the result of this fluctuation in thruster power. The change in plume emission maybe indicative of a change in plasma properties. This is supported by the performance measurements of Sankovic.[2]

This behavior suggests the duration and periodic nature of the transition between modes was affected by phenomena occurring on a time scale of minutes. While thermal effects and surface phenomena generally take place on these longer time scales no evidence as to the the actual mechanism was indicated by these data. Increasing the mass flow rate by 5 % increased the frequency of the periodic oscillation and the relative duration of the oscillatory mode. The increase in flow rate was accompanied by a small increase in discharge current. This periodic behavior was indicative of one series of tests and is not necessarily indicative of operation at any other time.

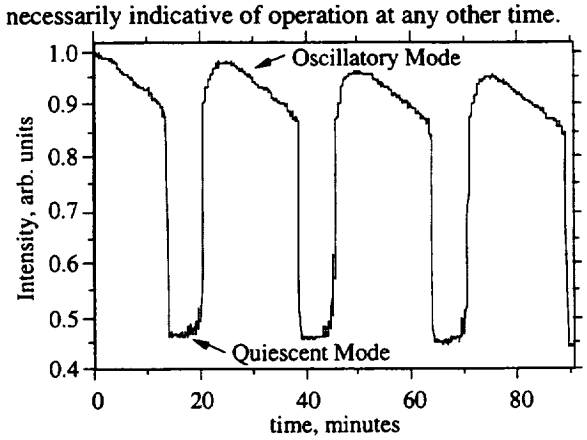

Figure 10a: Intensity of the 5419.2 Å Xe II Line vs. Time, flow rate 45.8 sccm.

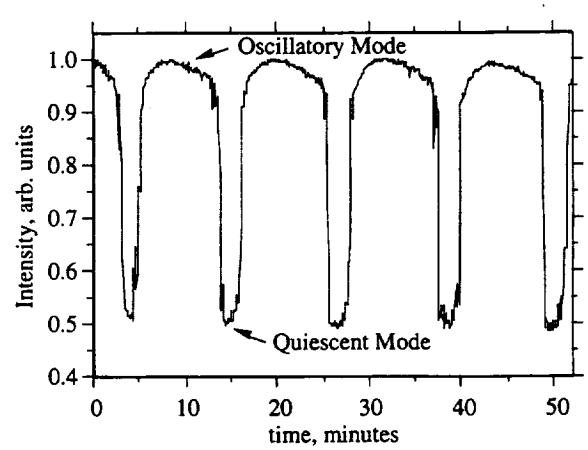

Figure 10b: Intensity of the 5419.2 Å Xe II Line vs. Time, flow rate 47.9 sccm.

Concluding Remarks

The emission spectra from the xenon plasma produced by a Russian SPT-100 was measured from 3000 to 9000 Å using a scanning monochromator. Approximately 270 individual Xe I, Xe II, and Xe III transitions were identified. A total of 250 mW of radiated optical emission was extrapolated from measurements taken at the thruster exit plane. There was no evidence of erosion products in the emission signature. Tests conducted in a facility with an ambient environment of nitrogen at 10^{-4} Torr demonstrated that ingestion and ionization of the background gas was measurable. The distribution of excited states could be described by temperatures ranging from fractions of an eV to 4 eV with a high degree of uncertainty due to the non-equilibrium nature of this plasma. It was shown that a

collisional-radiative model will be required for a complete description of the measured emission spectra. Ionization fractions of above 95 % were estimated at the thruster exit plane. Between 10 and 20% of the ions may have been doubly charged. Two modes of operation were identified. The intensity of plasma emission increased by a factor two in the oscillatory mode. The transfer between the two modes of operation seems to be affected by thermal or surface phenomena.

Acknowledgements

The author would like to thank M.A. Cappelli for his contribution to the interpretation of these data. This work was supported by the Ballistic Missile Defense Organization's Office of Innovative Science and Technology.

References

1. Brophy, J.R., Barnett, J.W., Sankovic, J.M., and Barnhart, D.A., "Performance of the Stationary Plasma Thruster: SPT-100," AIAA-92-3155, July 1992.
2. Sankovic, J.M., Hamley, J.A., and Haag, T.W., "Performance Evaluation of the Russian SPT Thruster at NASA LeRC," IEPC-93-094, Sept. 1993.
3. Hamley, J.A., Hill, G.M., and Sankovic, J.M., "Power Electronics Development for the SPT-100 Thruster," IEPC-93-044, Sept. 1993.
4. Pencil, E.J., "Far-Field Plume Sputtering Characterization of the Stationary Plasma Thruster (SPT-100)," IEPC-93-098, Sept. 1993.
5 Myers, R.M. and Manzella, D.H., "Stationary Plasma Thruster Plume Characteristics," IEPC-93-096, Sept. 1993.
6. Bugrova, A.I., *et. al.*,"Physical Processes and Characteristics of Stationary Plasma Thrusters with Closed Electron Drift," IEPC-91-079, Oct. 1991.
7. Absalamov, S.K., *et. al.*, "Measurement of Plasma Parameters in the Stationary Plasma Thruster (SPT-100) Plume and its Effect on Spacecraft Components,"`AIAA-92-3156, July 1992.
8. Komurasaki, K., Hirakawa, M., and Arakawa, Y., "Plasma Acceleration Process in a Hall-Current Thruster," IEPC-91-078, Oct. 1991.
9. Bugrova, A.I., Versotskii, V.S., Kalikhman, L.E., and Morozov, A.I., "Experimental Determination of the Electron Distribution Function in a Plasma Stream," *Teplofiz. Vys. Temp.*, Vol.16, No.5, Sept. 1978, p.937.
10. Bishaev, A.I., Versotskii, V.S., Kalikhman, L.E., and Morozov, A.I., "Experimental Determination of the Electron Distribution in a Plasma Stream," *Teplofiz. Vys. Temp.*, Vol.16, No.5, Sept. 1978, p.937.
11. Morozov, A.I., *et. al.*, "Plasma Accelerator with Closed Electron Drift and Extended Acceleration Zone," *Sov. Phys. Tech. Phys.*, Vol.17, No.1, July 1972, p.38.
12. Zubkov, I.P., Kislov, A.Y., Lebedev, S.V., and Morozov, A.I., "Ion Motion in a Double-Lens Accelerator with Closed Electron Drift," *Sov. Phys. Tech. Phys.*, Vol.16, No.3, Sept. 1971, p.409.
13. Bugrova, A.I., Morozov, A.I., and Kharchevnikov, V.K., "Probe Measurements of Drift Current in a Hall Accelerator," *Sov. Phys. Tech. Phys.*, Vol.30, No.6, June 1985, p.610.
14. Bugrova, A.I., Morozov, A.I., and Kharchevnikov, V.K., "Structural Studies of Boundary Layers by Probes of Various Diameters," *Sov. Phys. Tech. Phys.*, Vol.30, No.6, June 1985, p.612.
15. Bugrova, A.I., *et. al.*, Dynamics of the Electron Energy Distribution Function in a Plasma Accelerator with Extended Acceleration Zone," *Teplofiz. Vys. Temp.*, Vol. 19, No.6, Nov. 1981, p.1149.
16. Morozov, A.I., Bugrova, A.I., Ermolenko, V.A., and Lein, L.A., "A Study of Ion Formation in a Hall Accelerator," *Sov. Phys. Tech. Phys.*, Vol 33, No.2, Feb. 1988, p.185.
17. Bugrova, A.I. Daneliya, I.A., Ermolenko, V.A., and Kalikhman, L.E., "Electron Temperature in the Plasma Stream From a Hall Accelerator," *Sov. Phys. Tech. Phys.*, Vol.22, No.11, Nov. 1977, p.1337.
18. Cappelli, M.A., *et. al.*, "Sodium Atom Distribution Within a Heat Sandwich Oven," *Rev. Sci. Instrum.*, Vol. 56, No.11, 1985, p. 2030.
19. Vincenti, W.G., and Kruger, C.H., *Introduction to Physical Gas Dynamics*, Wiley, New York, 1967, p.108.
20. Small-Warren, N.E. and Chow Chiu, L.Y., "Lifetime of the Metastable $^3P_2$ and $^3P_0$ States of Rare-Gas Atoms," *Phys. Rev. A*, Vol. 11, No.6, 1975, p.1777.
21. Hoskins, W.A., Kull, A.E., and Butler G.W., "Measurements of Population and Temperature Profiles in an Arcjet Plume," AIAA-92-3240, July 1992.
22. Moore, C.E.,"Atomic Energy Levels, Volume III," United States National Bureau of Standards Circular 467, 1958.
23. Bober, A.S., "State of Work on Electrical Thrusters in USSR," IEPC-91-003, Oct.1991.
24. Personal communication: Tom Randolh, Space Systems/Loral.
25. Larrabee, R.D., "Spectral Emissivity of Tungsten," J. Opt. Soc. Am., Vol. 49, No. 6, 1959, p. 619.
26. Striganov, A.R. and Sventitskii, N.S., *Tables of Spectral Lines of Neutral and Ionized Atoms*, (translation from Russian) IFI/Plenum, New York 1968.
27 Wiese, W.L. and Martin, G.A., "Wavelengths and Transition Probabilities for Atoms and Atomic Ions, Part II: Transition Probabilities," United States National Bureau of Standards NSRDS-NBS 68, 1980.
28 Sadeghi, N. and Sabbagh, J., "Collisional Transfer Between the $6s'[1/2]_{0,1}$ and $6p[1/2]_1$ Xenon Levels," *Phys Rev A*, Vol 6, No 6, 1977, p 2336.

29 Miller, M.H., Roig, R.A., and Bengston, R.D., "Transition Probabilities of XeI and XeII," *Phys Rev A*, Vol 8, No 1, 1973, p 480.

30 Lazovskaya, V.R. and Tumakaev, G.K., "Shock Tube Measurements of the Oscillator Strengths and Stark Constants for s-p Transitions in Atomic Xenon," *Sov Phys Tech Phys*, Vol 24, No 3, 1979, p 328.

31. Peraza, C., Martin, P., and Campos, J., "Transition Probabilities of 6p-ns (n=7,8,9,10,11,12,13) Lines of Xe(I)," *JQSRT*, Vol 46, 1991, p 455.

32. Martin, P., Cabrera, J.A., and Campos, J., "Transition Probabilities of 6p-nd (n=7,8,9) Lines of XeI," *Phys Rev A*, Vol 32, No 5, 1985, p 3110.

Appendix A

Table AI: Xenon II Transitions and Physical Constants including measured values of $n_k L/ g_k$
Energy levels from Ref. 22, Uncertainties:A<25%, B<30%, C<40%, D<50%, E>50%

No	Transition		λ, (Å)	g_i	g_k	E_i,cm^{-1}	E_k,cm^{-1}	A_{ik}, (10^8s^{-1})	f_{ik}	ref	unc	$n_k L/ g_k$
1	$5p^45d\ ^4P_{1/2}$	- $5p^46p'\ ^2P_{1/2}$	3869.6	2	2	106906	132741	0.25	0.0561	29	E	18525
2	$5p^46p'\ ^2F_{5/2}$	- $5p^46d'\ ^2F_{5/2}$	3972.6	6	6	128867	154032	0.84	0.1987	29	D	651
3	$5p^46p\ ^4P_{1/2}$	- $5p^44f\ 20_{1/2}$	3990.3	2	2	113673	138726	0.40	0.0955	29	E	5333
4	$5p^46p\ ^4P_{5/2}$	- $5p^46d\ ^4F_{7/2}$	4057.5	6	8	111959	136598	0.22	0.0724	29	B	3399
5	$5p^46p\ ^4P_{3/2}$	- $5p^46d\ ^4D_{3/2}$	4180.1	4	4	111792	135708	0.42	0.1100	29	A	13866
6	$5p^46p\ ^4P_{5/2}$	- $5p^46d\ ^4D_{3/2}$	4209.5	6	4	111959	135708	0.54	0.0956	29	B	6706
7	$5p^46p\ ^2P_{3/2}$	- $5p^47s'\ 14_{5/2}$	4223.0	4	6	123255	146928	1.48	0.5935	29	B	1256
8	$5p^46p\ ^4P_{5/2}$	- $5p^46d\ ^4D_{5/2}$	4238.3	6	6	111959	135547	0.91	0.2451	29	A	2570
9	$5p^46p\ ^4P_{5/2}$	- $5p^46d\ ^4D_{7/2}$	4245.4	6	8	111959	135507	0.74	0.2666	29	B	5285
10	$5p^46p\ ^2P_{1/2}$	- $5p^46d'\ ^2D_{3/2}$	4251.6	2	4	124571	148085	1.33	0.7209	29	B	1613
11	$5p^46p\ ^4P_{3/2}$	- $5p^47s\ ^4P_{1/2}$	4296.4	4	2	111792	135061	0.72	0.0996	29	A	4986
12	$5p^46p\ ^2D_{5/2}$	- $5p^47s'\ ^2D_{5/2}$	4310.5	6	6	123113	146305	0.49	0.1365	29	B	2629
13	$5p^46p\ ^4D_{5/2}$	- $5p^46d\ ^4F_{7/2}$	4330.5	6	8	113512	136598	1.29	0.4836	29	A	2984
14	$5p^46p\ ^4P_{1/2}$	- $5p^46d\ 18_{1/2}$	4369.2	2	2	113673	136554	1.01	0.2891	29	A	2769
15	$5p^46p\ ^4D_{3/2}$	- $5p^46d\ ^4F_{3/2}$	4373.8	4	4	116783	139640	0.32	0.0918	29	B	2971
16	$5p^46p\ ^2P_{3/2}$	- $5p^46d\ ^2D_{3/2}$	4406.9	4	4	123255	145940	0.62	0.1805	29	B	2248
17	$5p^45d\ ^2D_{5/2}$	- $5p^46p'\ ^2D_{3/2}$	4470.9	6	4	109563	131924	0.10	0.0200	29	C	11108
18	$5p^46p\ ^4D_{3/2}$	- $5p^46d\ ^4F_{5/2}$	4480.9	4	6	116783	139094	1.33	0.6005	29	A	1534
19	$5p^46s'\ ^2D_{5/2}$	- $5p^46p'\ ^2F_{7/2}$	4532.5	6	8	108007	130064	0.21	0.0862	29	A	9265
20	$5p^46p\ ^2D_{3/2}$	- $5p^47s'\ ^2D_{5/2}$	4540.9	4	6	124290	146305	1.41	0.6538	29	A	945
21	$5p^46p\ ^4D_{3/2}$	- $5p^44f\ 20_{1/2}$	4555.9	4	2	116783	138726	0.57	0.0887	29	E	2650
22	$5p^46p\ ^4S_{3/2}$	- $5p^46d\ ^4P_{5/2}$	4592.1	4	6	121629	143399	0.89	0.4220	29	B	1873
23	$5p^46s\ ^4P_{3/2}$	- $5p^46p\ ^4D_{3/2}$	4603.0	4	4	95064	116783	0.69	0.2192	29	A	57872
24	$5p^46s\ ^2P_{3/2}$	- $5p^46p\ ^2D_{3/2}$	4651.9	4	4	102799	124290	0.35	0.1136	29	A	10690
25	$5p^46p\ ^4D_{3/2}$	- $5p^44f\ 12_{3/2}$	4698.0	4	4	116783	138063	1.29	0.4269	29	B	1894
26	$5p^46p\ ^2S_{1/2}$	- $5p^47s\ ^2P_{3/2}$	4715.2	2	4	121180	142382	0.57	0.3800	29	C	2874
27	$5p^45d\ ^2D_{3/2}$	- $5p^46p'\ ^2F_{5/2}$	4769.1	4	6	107905	128867	0.20	0.1023	29	B	8486
28	$5p^45d''\ ^2D_{5/2}$	- $5p^44f\ 15_{5/2}$	4773.2	6	6	119086	140030	0.25	0.0854	29	C	3136
29	$5p^45d'\ ^2D_{3/2}$	- $5p^46p'\ ^2D_{5/2}$	4787.8	4	6	111327	132208	0.22	0.1134	29	C	4930
30	$5p^45d\ ^4D_{3/2}$	- $5p^46p\ ^4D_{3/2}$	4818.0	4	4	96033	116783	0.12	0.0418	29	C	39096
31	$5p^46p\ ^4P_{3/2}$	- $5p^47s\ ^4P_{5/2}$	4823.4	4	6	111792	132519	0.49	0.2564	29	A	2703
32	$5p^46s\ ^4P_{5/2}$	- $5p^46p\ ^4D_{7/2}$	4844.3	6	8	93068	113705	0.77	0.3612	29	A	1986
33	$5p^46p\ ^4P_{5/2}$	- $5p^47s\ ^4P_{5/2}$	4862.5	6	6	111959	132519	0.72	0.2552	29	A	4849
34	$5p^45d\ ^2D_{5/2}$	- $5p^46p'\ ^2F_{7/2}$	4876.5	6	8	109563	130064	0.94	0.4468	29	A	8016
35	$5p^45d\ ^2D_{5/2}$	- $5p^46p'\ ^2P_{3/2}$	4972.7	6	4	109563	129667	0.96	0.2373	29	B	17838
36	$5p^46s\ ^2P_{1/2}$	- $5p^46p\ ^2D_{3/2}$	4988.7	2	4	104250	124290	0.35	0.2612	29	B	8695
37	$5p^46p\ ^4D_{5/2}$	- $5p^47s\ ^4P_{3/2}$	5080.6	6	4	113512	133189	1.70	0.4386	29	B	1915
38	$5p^45d'\ ^2D_{5/2}$	- $5p^46p'\ ^2D_{5/2}$	5125.7	6	6	112704	132208	0.54	0.2127	29	E	2257
39	$5p^45d\ ^2D_{5/2}$	- $5p^46p'\ ^2F_{5/2}$	5178.8	6	6	109563	128867	0.42	0.1689	29	E	3055
40	$5p^46s\ ^4P_{5/2}$	- $5p^46p\ ^4P_{5/2}$	5292.2	6	6	93068	111959	2.32	0.9471	29	A	8194
41	$5p^46s\ ^4P_{5/2}$	- $5p^46p\ ^4P_{3/2}$	5339.4	6	4	93068	111792	1.88	0.5357	29	B	6092
42	$5p^46s\ ^4P_{3/2}$	- $5p^46p\ ^4D_{5/2}$	5419.2	4	6	95064	113512	2.13	1.4607	29	B	10053
43	$5p^46s\ ^2P_{3/2}$	- $5p^46p\ ^2S_{1/2}$	5439.0	4	2	102799	121180	3.76	0.8338	29	B	2870
44	$5p^45d\ ^2P_{1/2}$	- $5p^46p\ ^2D_{3/2}$	5450.5	2	4	105948	124290	0.37	0.3296	29	D	3794
45	$5p^45d\ ^4D_{5/2}$	- $5p^46p\ ^4D_{7/2}$	5460.4	6	8	95397	113705	0.27	0.1609	29	B	3255
46	$5p^45d\ ^4D_{7/2}$	- $5p^46p\ ^4D_{7/2}$	5472.6	8	8	95438	113705	0.49	0.2200	29	B	3466
47	$5p^45d\ ^4D_{7/2}$	- $5p^46p\ ^4D_{5/2}$	5531.1	8	6	95438	113512	0.12	0.0413	29	C	23154
48	$5p^45d\ ^2P_{3/2}$	- $5p^46p\ ^2D_{5/2}$	5616.7	4	6	105313	123113	0.35	0.2483	29	C	2147
49	$5p^45d\ ^2P_{1/2}$	- $5p^46p\ ^2P_{1/2}$	5659.4	2	2	105948	124571	1.30	0.6242	29	D	3763
50	$5p^45d\ ^4D_{3/2}$	- $5p^46p\ ^4P_{1/2}$	5667.6	4	2	96033	113673	1.23	0.2962	29	C	5967
51	$5p^45d'\ ^2D_{3/2}$	- $5p^46p'\ ^2F_{5/2}$	5699.6	4	6	111327	128867	0.74	0.5406	29	C	1577
52	$5p^45d\ ^4P_{1/2}$	- $5p^46p\ ^2D_{3/2}$	5751.0	2	4	106906	124290	1.06	1.0512	29	C	3093

53	$5p^45d'\ ^2D_{5/2}$	-	$5p^46p'\ ^2F_{7/2}$	5758.7	6	8	112704	130064	0.94	0.6231	29	C	1354
54	$5p^45d\ ^2P_{1/2}$	-	$5p^46p\ ^2P_{3/2}$	5776.4	2	4	105948	123255	0.61	0.6103	29	D	4115
55	$5p^45d'\ ^2D_{5/2}$	-	$5p^46p'\ ^2P_{3/2}$	5893.3	6	4	112704	129667	1.16	0.4027	29	E	3876
56	$5p^46s'\ ^2D_{3/2}$	-	$5p^46p'\ ^2P_{3/2}$	5971.1	4	4	112925	129667	1.30	0.6949	29	E	2518
57	$5p^46s\ ^4P_{3/2}$	-	$5p^46p\ ^4P_{3/2}$	5976.5	4	4	95064	111792	1.09	0.5837	29	D	3861
58	$5p^45d\ ^4D_{5/2}$	-	$5p^46p\ ^4P_{5/2}$	6036.2	6	6	95397	111959	0.15	0.0819	29	C	11705
59	$5p^45d\ ^4D_{7/2}$	-	$5p^46p\ ^4P_{5/2}$	6051.2	8	6	95438	111959	0.52	0.2141	29	D	6833
60	$5p^45d\ ^4D_{5/2}$	-	$5p^46p\ ^4P_{3/2}$	6097.6	6	4	95397	111792	0.72	0.2676	29	B	5427
61	$5p^46s'\ ^2D_{3/2}$	-	$5p^46p'\ ^2F_{5/2}$	6270.8	4	6	112925	128867	0.89	0.7870	29	E	3288
62	$5p^45d\ ^4D_{3/2}$	-	$5p^46p\ ^4P_{5/2}$	6277.5	4	6	96033	111959	0.15	0.1329	29	E	7260
63	$5p^45d\ ^2P_{3/2}$	-	$5p^46p\ ^2S_{1/2}$	6300.9	4	2	105313	121180	0.62	0.1845	29	E	2627
64	$5p^45d\ ^4D_{3/2}$	-	$5p^46p\ ^4P_{3/2}$	6344.0	4	4	96033	111792	0.82	0.4948	29	E	1659
65	$5p^45d\ ^2P_{1/2}$	-	$5p^46p\ ^4S_{3/2}$	6375.3	2	4	105948	121629	0.62	0.7556	29	E	717
66	$5p^45d\ ^2D_{3/2}$	-	$5p^46p\ ^2P_{3/2}$	6512.8	4	4	107905	123255	0.49	0.3116	29	E	4813
67	$5p^45d'\ ^2F_{5/2}$	-	$5p^46p'\ ^2F_{7/2}$	6528.7	6	8	114751	130064	0.42	0.3579	29	E	1421
68	$5p^45d\ ^4D_{1/2}$	-	$5p^46p\ ^4P_{3/2}$	6694.3	2	4	96858	111792	0.62	0.8331	29	D	1745
69	$5p^45d\ ^4F_{7/2}$	-	$5p^46p\ ^4D_{5/2}$	6805.7	8	6	98823	113512	0.061	0.0318	27	D	34818
70	$5p^45d\ ^2P_{1/2}$	-	$5p^46p\ ^4D_{1/2}$	6910.2	2	2	105948	120415	0.20	0.1432	29	E	11130
71	$5p^45d\ ^4F_{3/2}$	-	$5p^46p\ ^4D_{7/2}$	6990.9	4	8	99405	113705	0.27	0.3957	29	C	12572
72	$5p^45d'\ ^2F_{7/2}$	-	$5p^46p'\ ^2F_{5/2}$	7164.8	8	6	114914	128867	0.69	0.3983	29	E	1132

Table A2: Xenon I Transitions and Physical Constants including measured values of n_kL/g_k
Energy levels from Ref. 22, Uncertainties: A<10%, B<25%, C<40%, D<50%, E>50%

No	Transition			λ, (Å)	g_i	g_k	E_i,cm^{-1}	E_k,cm^{-1}	A_{ik}, ($10^8 s^{-1}$)	f_{ik}	ref	unc	n_kL/g_k
1	$5p^56s[3/2]_1$	-	$5p^58p[1/2]_0$	4078.8	3	1	68046	92556	0.0049	0.0004	27	C	1482887
2	$5p^56s[3/2]_2$	-	$5p^56p'[1/2]_1$	4501.0	5	3	67068	89279	0.0039	0.0007	27	C	295386
3	$5p^56s[3/2]_2$	-	$5p^56p'[3/2]_2$	4524.7	5	5	67068	89163	0.0021	0.0006	28	D	2340427
4	$5p^56s[3/2]_1$	-	$5p^56p'[1/2]_0$	4582.7	3	1	68046	89861	0.0039	0.0004	27	C	3655830
5	$5p^56s[3/2]_1$	-	$5p^56p'[3/2]_2$	4734.2	3	5	68046	89163	0.0009	0.0005	27	C	1655900
6	$5p^56s[3/2]_2$	-	$5p^57p[3/2]_2$	4624.3	5	5	67068	88687	0.0042	0.0013	27	C	1093916
7	$5p^56s[3/2]_1$	-	$5p^57p[1/2]_0$	4807.0	3	1	68046	88843	0.0152	0.0018	27	C	700020
8	$5p^56s[3/2]_1$	-	$5p^57p[3/2]_1$	4829.7	3	3	68046	88745	0.0019	0.0007	27	C	1140458
9	$5p^56p[3/2]_2$	-	$5p^59d[3/2]_2$	6224.2	5	5	79213	95275	0.0129	0.0075	32		37243
10	$5p^56p[1/2]_1$	-	$5p^59d[1/2]_1$	5566.6	1	3	77270	95229	0.0290	0.0405	32		24031
11	$5p^56p[1/2]_1$	-	$5p^59d[1/2]_0$	5581.8	3	1	77270	95180	0.0312	0.0049	32		138501
12	$5p^56p[5/2]_2$	-	$5p^510s[3/2]_1$	5998.1	5	3	78120	94788	0.0058	0.0019	31	A	94966
13	$5p^56p[5/2]_2$	-	$5p^59d[5/2]_2$	5814.5	5	5	78120	95314	0.0093	0.0047	32		54066
14	$5p^56p[1/2]_1$	-	$5p^58d[3/2]_2$	5875.0	3	5	77270	94286	0.0242	0.0208	32		38154
15	$5p^56p[3/2]_1$	-	$5p^58d[3/2]_2$	6521.5	3	5	78957	94286	0.0023	0.0024	32		126856
16	$5p^56p[3/2]_2$	-	$5p^58d[3/2]_2$	6632.4	5	5	79213	94286	0.0194	0.0128	32		34957
17	$5p^56p[3/2]_1$	-	$5p^58d[3/2]_1$	6355.8	3	3	78957	94686	0.0204	0.0123	32		108339
18	$5p^56p[5/2]_3$	-	$5p^58d[5/2]_3$	6261.2	7	7	78404	94371	0.0137	0.0080	32		15871
19	$5p^56p[5/2]_3$	-	$5p^58d[7/2]_3$	6292.4	7	7	78404	94291	0.0023	0.0013	32		142792
20	$5p^56p[5/2]_2$	-	$5p^59s[3/2]_1$	6533.2	5	3	78120	93423	0.0103	0.0040	31	A	134478
21	$5p^56p[3/2]_1$	-	$5p^59s[3/2]_1$	6910.8	3	3	78957	93423	0.0074	0.0053	31	A	201293
22	$5p^56p[1/2]_1$	-	$5p^59s[3/2]_2$	6198.3	3	5	77270	93399	0.0066	0.0063	31	A	112284
23	$5p^56p[5/2]_3$	-	$5p^58d[7/2]_4$	6318.1	7	9	78404	94227	0.0270	0.0208	27	C	46356
24	$5p^56p[5/2]_2$	-	$5p^57d[3/2]_2$	6846.6	5	5	78120	92722	0.0003	0.0002	32		4384868
25	$5p^56p[3/2]_1$	-	$5p^57d[5/2]_2$	7285.3	3	5	78957	92679	0.0409	0.0542	32		28473
26	$5p^56p[5/2]_3$	-	$5p^57d[5/2]_3$	6976.2	7	7	78404	92734	0.0191	0.0139	32		47805
27	$5p^56p[3/2]_2$	-	$5p^57d[5/2]_3$	7393.8	5	7	79213	92734	0.0489	0.0561	32		13417
28	$5p^56p[5/2]_2$	-	$5p^57d[7/2]_3$	6882.2	5	7	78120	92647	0.0640	0.0636	27	D	72024
29	$5p^56p[5/2]_3$	-	$5p^57d[7/2]_4$	7119.6	7	9	78404	92445	0.0660	0.0645	28	D	18368
30	$5p^56p[1/2]_1$	-	$5p^58s[3/2]_2$	7386.0	3	5	77270	90805	0.0125	0.0170	31	A	39936
31	$5p^56s'[1/2]_1$	-	$5p^56p'[1/2]_0$	7887.4	3	1	77186	89861	0.0104	0.0032	27	D	4709937
32	$5p^56s'[1/2]_1$	-	$5p^56p'[3/2]_2$	8346.8	3	5	77186	89163	0.0636	0.1107	27	C	239879
33	$5p^56s'[1/2]_0$	-	$5p^57p[3/2]_1$	7967.3	1	3	76197	88745	0.0030	0.0086	28	D	1266150
34	$5p^56s[3/2]_2$	-	$5p^56p[3/2]_2$	8231.6	5	5	67068	79213	0.038	0.0386	27	C	2424880
35	$5p^56s[3/2]_1$	-	$5p^56p[1/2]_0$	8280.1	3	1	68046	80119	0.100	0.0343	27	C	24424003
36	$5p^56s[3/2]_2$	-	$5p^56p[3/2]_1$	8409.2	5	3	67068	78957	0.0083	0.0053	27	C	705646
37	$5p^56s[3/2]_2$	-	$5p^56p[5/2]_3$	8819.4	5	7	67068	78404	0.276	0.4500	30	B	610047

REPORT DOCUMENTATION PAGE

Form Approved
OMB No. 0704-0188

Public reporting burden for this collection of information is estimated to average 1 hour per response, including the time for reviewing instructions, searching existing data sources, gathering and maintaining the data needed, and completing and reviewing the collection of information. Send comments regarding this burden estimate or any other aspect of this collection of information, including suggestions for reducing this burden, to Washington Headquarters Services, Directorate for Information Operations and Reports, 1215 Jefferson Davis Highway, Suite 1204, Arlington, VA 22202-4302, and to the Office of Management and Budget, Paperwork Reduction Project (0704-0188), Washington, DC 20503.

1. AGENCY USE ONLY (*Leave blank*)

2. REPORT DATE
March 1994

3. REPORT TYPE AND DATES COVERED
Final Contractor Report

4. TITLE AND SUBTITLE
Stationary Plasma Thruster Plume Emissions

5. FUNDING NUMBERS
WU-506-42-31
C-NAS3-25266

6. AUTHOR(S)
David H. Manzella

7. PERFORMING ORGANIZATION NAME(S) AND ADDRESS(ES)
Sverdrup Technology, Inc.
Lewis Research Center Group
2001 Aerospace Parkway
Brook Park, Ohio 44142

8. PERFORMING ORGANIZATION REPORT NUMBER
E-8612

9. SPONSORING/MONITORING AGENCY NAME(S) AND ADDRESS(ES)
National Aeronautics and Space Administration
Lewis Research Center
Cleveland, Ohio 44135-3191

10. SPONSORING/MONITORING AGENCY REPORT NUMBER
NASA CR-194471
IEPC-93-097

11. SUPPLEMENTARY NOTES
Prepared for the 23rd International Electric Propulsion Conference sponsored by the American Institute of Aeronautics and Astronautics, Seattle, Washington, September 13-16, 1993. David H. Manzella presently at NYMA, Inc., Engineering Services Division, 2001 Aerospace Parkway, Brook Park, Ohio 44142. Project Manager, Francis M. Curran, Space Propulsion Technology Division, organization code 5330, NASA Lewis Research Center, (216) 433-7424.

12a. DISTRIBUTION/AVAILABILITY STATEMENT
Unclassified - Unlimited
Subject Category 20

12b. DISTRIBUTION CODE

13. ABSTRACT ***(Maximum 200 words)***
The emission spectrum from a xenon plasma produced by a Stationary Plasma Thruster provided by the Ballistic Missile Defense Organization (BMDO) was measured. Approximately 270 individual Xe I, Xe II, and XE III transitions were identified. A total of 250 mW of radiated optical emission was estimated from measurements taken at the thruster exit plane. There was no evidence of erosion products in the emission signature. Ingestion and ionization of background gas at elevated background pressure was detected. The distribution of excited states could be described by temperatures ranging from fractions of 1 eV to 4 eV with a high degree of uncertainty due to the nonequilibrium nature of this plasma. The plasma was over 95% ionized at the thruster exit plane. Between 10 and 20% of the ions were doubly charged. Two modes of operation were identified. The intensity of plasma emission increased by a factor of two during operation in an oscillatory mode. The transfer between the two modes of operation was likely related to unidentified phenomena occurring on a time scale of minutes.

14. SUBJECT TERMS
Stationary plasma thruster; Emission spectroscopy; Xenon

15. NUMBER OF PAGES
13

16. PRICE CODE
A03

17. SECURITY CLASSIFICATION OF REPORT
Unclassified

18. SECURITY CLASSIFICATION OF THIS PAGE
Unclassified

19. SECURITY CLASSIFICATION OF ABSTRACT
Unclassified

20. LIMITATION OF ABSTRACT